Tan, CM., Nix, AR., & Beach, MA. (2002). Dynamic spatial-temporal propagation measurement and super-resolution channel characterisation at 5.2 GHz in a corridor environment. *IEEE 56th Vehicular Technology Conference, 2002 (VTC 2002-Fall)*, *2*, 797 - 801. https://doi.org/10.1109/VETECF.2002.1040709

Dynamic spatial-temporal propagation measurement and super-resolution channel characterisation at 5.2GHz in a corridor environment

C. M. Tan, A. R. Nix, M. A. Beach

Centre for Communications Research
Merchant Venturers Building, University of Bristol,
Bristol BS8 1UB, UK.
Email: Chor.Min.Tan@bristol.ac.uk

Abstract*—This paper presents the analysed results from a dynamic spatial-temporal measurement campaign conducted at 5.2 GHz in a corridor environment within a modern building. The Single-Input-Multiple-Output (SIMO) measurement was performed by moving the transmitting antenna with a specialised trolley along a predefined route, while the receiving linear array was fixed at one location. Subsequent post-processing was conducted using the 2-D Unitary ESPRIT (Estimation of Signal Parameters via Rotational Invariance Techniques) super-resolution algorithm to extract the direction-of-arrival (DoA) and time-delay-of-arrival (TDoA) of the multipath components. The corridor was then characterised in terms of delay spread, azimuth spread, K-factor and coherence bandwidth. It was found that the corridor favours a wave-guiding effect whereas locations adjacent to the corridor enjoy the leakage of energy from the waves propagating along the corridor. The dynamic power delay spectrums are shown. Finally, the correlations between the delay spread, azimuth spread and coherence bandwidth are assessed.

***Keywords*—direction-of-arrival; propagation measurement; corridor; ESPRIT; channel characterisation**

I. INTRODUCTION

In order to fulfill the requirements of higher data rates and capacities for future indoor wireless communications, both HIPERLAN/2 and IEEE 802.11a have been standardised in the 5 GHz band. Numerous research programmes are now underway and are focused on evaluating and characterising the wireless channel so that proper radio architectures with smart antenna technology can be designed and implemented efficiently. This requires a well-planned channel sounding activity using state-of-the-art post-processing tools to aid the subsequent channel evaluation process.

Despite a considerable number of references in the area of channel sounding, very few of them fully address channel behavior in terms of the spatial, temporal, and frequency domains. To date, most measurements support analysis of channel time dispersion, frequency selectivity and power envelope variations since these are crucial for existing communication systems. However, for future wideband wireless systems ultilising smart antenna technology, supplemental information such as the direction-of-arrival (DoA), multipath clusterings, dynamic evolution of multipaths, etc, are needed. Hence, an appropriate multi-dimensional (m-D) channel sounding campaign must be performed to enable the aforementioned analysis to be conducted. In addition, special signal processing techniques based on multi-dimensional super-resolution algorithms must be developed to support the subsequent data processing in order to guarantee accuracy.

This paper describes the dynamic Single-Input-Multiple-Output (SIMO) wideband measurements conducted at 5.2 GHz in an indoor corridor environment. The 2-D Unitary ESPRIT (Estimation of Signal Parameters via Rotational Invariance Techniques) [1] algorithm was used to extract the direction-of-arrival (DoA) and time-delay-of-arrival (TDoA) of the multipath components. The corridor was characterised in terms of the delay spread, azimuth spread, K-factor and coherence bandwidth. It was found that the corridor favours a wave-guiding effect in line-of-sight (LOS) conditions, while locations adjacent to the corridor (NLOS) are supported by the leakage of energy from the waves propagating along the corridor.

This paper is organised as follows. Section 2 describes the measurement setup and the corridor environment. Section 3 presents the analysed results. Finally, Section 4 concludes the paper.

II. DYNAMIC MEASUREMENT SETUP AND DESCRIPTION OF THE ENVIRONMENT

A. Measurement equipment and setup

The SIMO measurement was conducted using a Medav RUSK BRI [2] channel sounder operating at 5.2 GHz. A periodic multitone signal with a bandwidth of 120 MHz and repetition period of 0.8 μs was employed in each case. The frequency domain channel response was calculated online and stored on the sounder's hard disk for post-processing. The mobile transmitter (Tx) used an omni-directional antenna transmitting at an input power of +26 dBm with a stationary

receiver (Rx) comprising a uniform linear array (ULA). The ULA had 8 active dipole-like elements spaced by half a wavelength and 2 dummy elements at both ends to balance the mutual coupling effect. The effective azimuth visible range of the ULA is 120º. The height of the mobile Tx was fixed at 1.8 m, while the height of the stationary Rx was fixed at 1.8 m to simulate the mobile-to-mobile link (MS-MS) and 2.1 m to simulate the basestation-to-mobile link (BS-MS).

The dynamic measurements were conducted by slowly pushing the Tx towards the Rx using a trolley and telemetry equipment specially developed for this dynamic channel sounding exercise. The trolley had 2 odometers on the left and right wheels that enable precise logging of the distance moved. The telemetry apparatus consisted of a sending (Fig.1) and a receiving unit (Fig.2). This was used for transmitting the navigation data from the odometers on the mobile terminal (in our case the Tx) to the fixed receiving station (in our case the Rx).

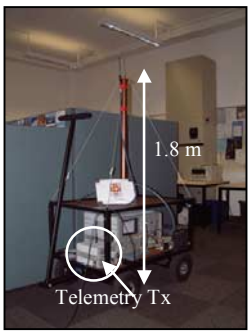

Figure 1. Medav RUSK BRI Tx and mobile trolley

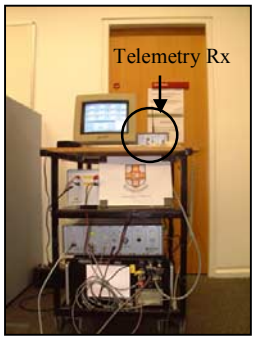

Figure 2. Medav RUSK BRI Rx – fixed receiving station

In a dynamic measurement campaign with distance mode setting, the sounder will record the channel response at every triggering event. The system is able to trigger 244 pulses every 1 m, which is equivalent to 14 pulses per wavelength (λ) at 5.2 GHz. Here, the sounder was configured to record 20 SIMO snapshots[1] consecutively for every 80 mm moved, i.e. a pulse was triggered every 80 mm. Since pushing the trolley in a precise straight path is impractical, the triggering event for recording 20 snapshots consecutively at every 80 mm was controlled by referring to only one of the odometers. For a test signal with excess delay window of 0.8 µs, the time for recording a full SIMO snapshot was 12.8 µs [2]. Therefore, the total recording time of 20 consecutive SIMO snapshots was 256 µs, which was well within the coherence time of the channel and also the 2 ms Medium Access Control (MAC) frame of the HIPERLAN/2 standard. Since the trolley was pushed at approximately 1 m/s, the distance moved when 1 SIMO snapshot was being recorded was $2.22 \times 10^{-4}\ \lambda$ (0.02% of λ). Therefore, the uncertainty introduced by the trolley movement in 1 SIMO snapshot was negligible.

[1] A SIMO snapshot consists of 8 complex channel response measurements in the frequency domain across the 8-element ULA.

B. *Indoor corridor environment*

The measurements were conducted in the summer of 2001 in a corridor environment in the Merchant Venturers Building of the University of Bristol (UK). Both LOS and NLOS conditions were considered, which formed part of the picocell scenarios in the European-COST 259 channel model [3]. Fig. 3 shows a sketched plan of the environment.

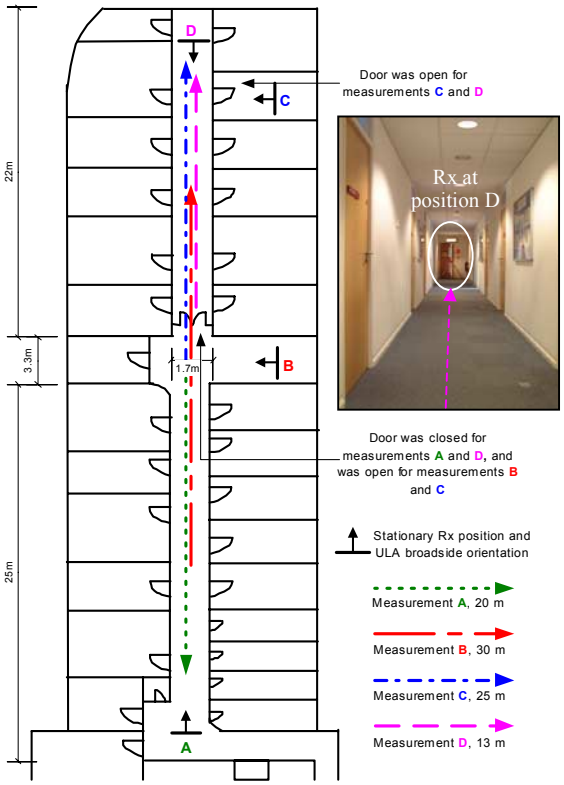

Figure 3. Sketched plan of the corridor environment

The walls along the corridor and between the rooms were made of plasterboard on an aluminum frame with wooden office doors, and the outer walls were made of brick and concrete. The floor was carpeted on metal sheets and the ceiling was covered with soft boards (approximately 20 mm gap between the 'visible' soft board ceiling and the concrete layer). The height of the corridor was 2.45 m. Several notice boards with metal frames surrounding plasterboard and glass sheets were located along both sides of the corridor.

The measurements conducted are indicated in different line styles (Fig. 3), representing different paths for the mobile Tx and the corresponding stationary Rx. LOS was achieved when the Rx was placed at positions 'A' and 'D', while positions 'B' and 'C' represented the NLOS scenarios (with the exception that LOS was achieved when the mobile Tx was pushed past the Rx). All measurements were conducted during normal office hours to emulate a realistic typical indoor environment. Hence, people were allowed to move around the corridor freely during the measurement period.

III. DATA PROCESSING AND CHANNEL CHARACTERISATION

A. *Super-resolution algorithm*

Since the channel response was stored in the frequency domain, one can simply apply the Inverse Fourier Transform (IFT) to obtain the power delay profile (PDP). Due to the finite sounding bandwidth, sidelobes will occur in the PDP and will superimpose with the mainlobe and sidelobes corresponding to a particular multipath component. Although applying a suitable window function can reduce the sidelobe levels, this is achieved at the cost of reduced time resolution and increased difficulty in resolving the closely spaced paths. On the other hand, a high sidelobe level will cause a 'phantom path' in the PDP as one might misinterpret it to be one of the multipaths in the channel that is in fact non-existent.

The super-resolution algorithms are ideally suited in multipath rich environments. Here, the 2-D Unitary ESPRIT algorithm [1] was used to extract the DoA and TDoA of the multipaths. A 2-D forward-backward spatial-temporal smoothing process was applied prior to ESPRIT in order to decorrelate any correlated components. ESPRIT is able to provide discrete channel parameters (DoA, TDoA) values as a closed-form solution that can simplify the subsequent channel evaluation process. The resolution of the ESPRIT algorithm is far greater than the Rayleigh resolution such that any closely spaced paths can be easily resolved provided that a high signal-to-noise ratio (SNR) and a large number of samples are taken within the coherence time of the channel. Resolution is further enhanced when the channel parameters in one domain (e.g. spatial or temporal) have a distinct value.

The end products of the 2-D Unitary ESPRIT algorithm are the DoA and TDoA values corresponding to a particular distance dependent channel response. The distance-variant complex impulse response is thus represented by:

$$h(d,\theta,\tau)=\sum_{l=1}^{L}\gamma_{d,l}B(\theta_{d,l})\cdot\delta(\theta-\theta_{d,l})\cdot\delta(\tau-\tau_{d,l}) \qquad (1)$$

where L is the total number of multipaths at a particular distance, d is the distance-dependent parameter, θ is the DoA, τ is the TDoA, B is the antenna beampattern, and γ is the complex path weight. Since the effective instantaneous dynamic range of the channel sounder is around 40 dB, any signal component with power weaker than 30 dB below the strongest component was rejected as noise. A full 40 dB cutoff threshold was not applied since ESPRIT is sensitive to the SNR and estimates will be unreliable in the case of poor SNR.

B. *Power Delay Profile (PDP)*

The distance-variant power azimuth delay profile is given by (2).

$$P(d,\theta,\tau)=\sum_{l=1}^{L}\left|\gamma_{d,l}\right|^2\delta(\theta-\theta_{d,l})\cdot\delta(\tau-\tau_{d,l}) \qquad (2)$$

The distance-variant power delay profile (3) can be obtained by integrating (2) with respect to θ.

$$P(d,\tau)=\int P(d,\theta,\tau)\ d\theta \qquad (3)$$

Fig. 4 shows the distance-variant PDP of the channel for the MS-MS link as the mobile trolley was pushed along the paths shown in Fig. 3. With walls up to the ceiling, the narrow corridor exhibits a wave-guiding effect where most of the signals arrived very shortly after the first component. For measurements 'A' and 'D', other than the strongest LOS component, most of the signal energy was guided to the Rx through multiple reflections along the walls, ceiling and floor. However, reflections along the ceiling and the floor are only observable if a 2-D array (such as a rectangular array) is used in the measurement (to support elevation angle estimation).

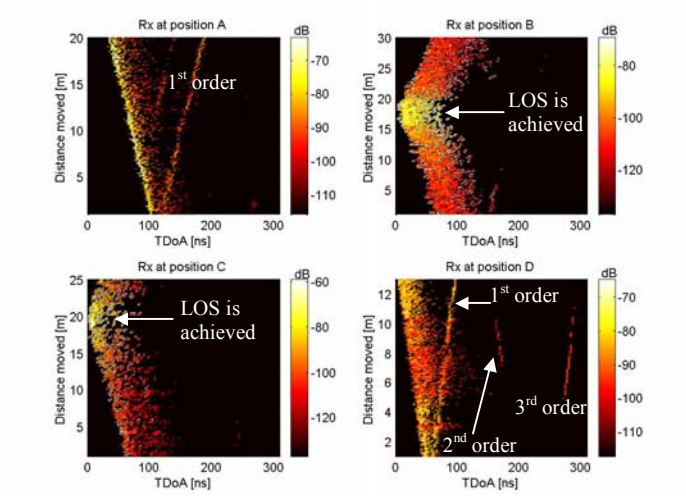

Figure 4. Distance-variant PDP for MS-MS link – Rx height of 1.8 m

Higher order reflections can be clearly seen in the PDP of measurement 'D'. Since the Tx antenna was omni-directional, in addition to travelling directly to the Rx ahead of the trolley, the signals also travel towards the closed wooden door in the middle of the corridor and are reflected back towards the Rx (1st order). This accounts for the increased TDoA for the 1st order reflection signals as the trolley approaches the Rx. It can also be seen that the signals travelling towards the Rx direction were reflected (1st order) back to the wooden door (in the middle of the corridor) by the wall behind the Rx, and then travel towards the Rx again after being reflected (2nd order) by the wooden door. This phenomena forms a 'line spectrum' which appears parallel to the strongest LOS component. The same argument applies to the 3rd order reflections in which its 'line spectrum' is parallel to the 1st order reflection components.

Since the trolley was pushed manually towards the Rx, there were some unavoidable human effects associated with the measurements. Some of the higher order reflections could not be extracted as their propagation paths were blocked by the person pushing the trolley. This causes a poor SNR in the obstructed components and the ESPRIT algorithm is then not able to resolve them.

For measurements 'B' and 'C', it can be seen that the power increases as the trolley moves past the Rx (LOS was achieved) and gradually decreases in the transition of LOS to NLOS. In NLOS condition, the multipaths arrive at the Rx through multiple reflections, diffractions, and scattering. This observation is consistent with that reported by Lafortune and Lecours [4], namely that when the Rx is placed in a location adjacent to a strong power zone (corridor in this case), the signals will arrive at the Rx through diffraction.

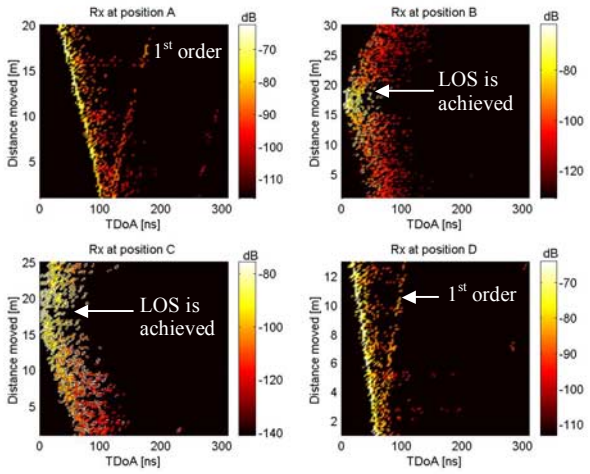

Figure 5. Distance-variant PDP for BS-MS link – Rx height of 2.1 m

Fig. 5 shows the PDP for the BS-MS link. It can be seen that the propagation mechanism in both configurations is very similar. However, the higher order reflections are less observable when the Rx is higher than the Tx. This is due to the directive antenna elements on both the terminals, which had their highest gain in the azimuth plane. Any signals arriving at an elevation angle experienced extra attenuation caused by the antenna effects and were thus less observable.

C. *K-factor*

Fig. 6 shows the cumulative distribution function (CDF) of the K-factor for all four propagation scenarios:

1. MS-MS LOS link – measurements 'A' and 'D', Rx height was 1.8 m
2. MS-MS NLOS link – measurements 'B' and 'C', Rx height was 1.8 m
3. BS-MS LOS link – measurements 'A' and 'D', Rx height was 2.1 m
4. BS-MS NLOS link – measurements 'B' and 'C', Rx height was 2.1 m

For more than 80% of the time the K-factor is negative. This suggests that the channel is not dominated by a strong component and implies that the reflected paths that are guided by the corridor have (relatively) strong power. The K-factors in the NLOS scenarios have lower values since diffraction and scattering play an important role in this case and the multipaths have similar power levels.

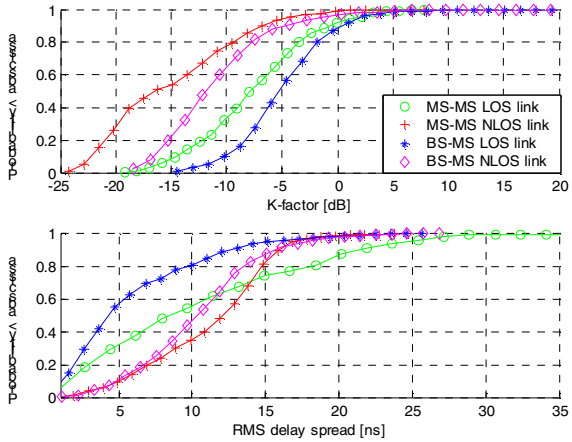

Figure 6. CDFs of the K-factor (top) and RMS delay spread (bottom)

D. *RMS delay spread*

RMS delay spread is the square root of the second central moment of the PDP and its CDF is shown at the bottom of Fig. 6. In general, NLOS scenarios have a larger delay spread than the LOS scenarios. Due to the significant higher order reflections with larger TDoA, the delay spread in the MS-MS LOS link is occasionally larger than that in the NLOS scenarios. Since the 2nd and 3rd order reflections are insignificant most of the time in the BS-MS LOS link it shows the smallest delay spread.

E. *RMS azimuth spread*

Similar to the RMS delay spread, the RMS azimuth spread is the square root of the second central moment of the power azimuth spectrum. As shown in Fig. 7, the azimuth spread seems to be unaffected by the heights of the Rx. Its distribution for the MS-MS and BS-MS links are very similar in their respective LOS and NLOS scenarios. For more than 50% of the time, the spread in LOS conditions is about 3 times that in NLOS conditions, indicating more spatial decorrelation between the ULA elements in NLOS conditions. The spread in LOS conditions is smaller since the waves are guided to the Rx along the narrow wave-guiding corridor. However, the height of the Rx seems to affect the correlation between the azimuth spread and delay spread – Table 1.

Table 1. Correlation coefficients of the azimuth spread and delay spread

Scenarios	LOS	NLOS
MS-MS link	0.57	0.58
BS-MS link	0.24	0.35

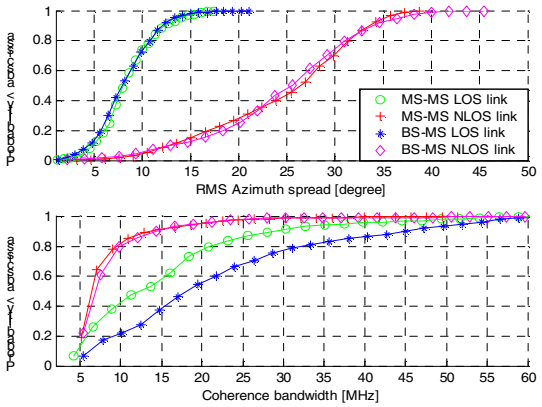

Figure 7. CDFs of the RMS azimuth spread (top) and coherence bandwidth (bottom)

F. Coherence bandwidth

Fig. 7 (bottom) shows the CDF of the coherence bandwidth (B_c) for a frequency correlation threshold (ρ) of 0.9. As expected, the NLOS scenarios have a lower coherence bandwidth compared to the LOS scenarios. For more than 90% of the time, the coherence bandwidth in NLOS condition never exceeds 15 MHz. This implies that the location adjacent to the corridor is highly selective in frequency. Since the higher order reflections in the BS-MS LOS link are insignificant, its channel is less frequency selective.

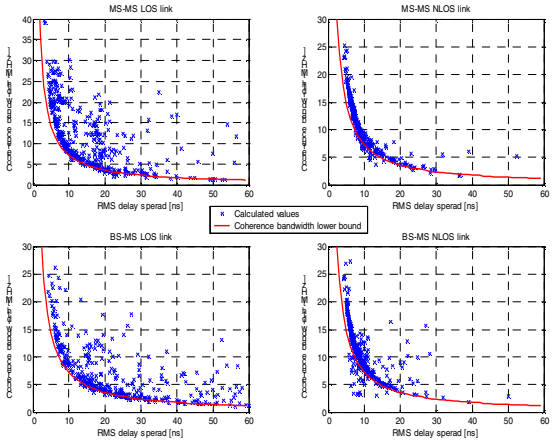

Figure 8. Scatter plots of the coherence bandwidth and RMS delay spread

Fig. 8 shows the scatter plot of the coherence bandwidth and the RMS delay spread (τ_{rms}), and their correlation coefficients are shown in Table 2. It can be concluded that both quantities are correlated. By assuming a wide-sense stationary uncorrelated scattering (WSSUS) channel, Fleury [5] has introduced the B_c lower bound value given by (4), and this is plotted as the solid curved line in Fig. 8. As shown, our analysis agrees very well with this theoretical lower bound limit.

Fitton et al. [6] reported that the presence of the low power paths at large TDoA will unduly affect the τ_{rms} values, while the B_c is largely unaffected in this case. This accounts for the behavior of the plots for the LOS scenarios in Fig. 8 in which the data points are more scattered compared to that in NLOS scenarios. This is due to the presence of higher order reflections at large TDoA in the LOS scenarios.

$$B_c(\rho) = \frac{\cos^{-1}(\rho)}{2\pi\tau_{rms}} \tag{4}$$

Table 2. Correlation coefficients of coherence bandwidth and delay spread

Scenarios	LOS	NLOS
MS-MS link	0.59	0.77
BS-MS link	0.60	0.61

IV. CONCLUSIONS

It is observed that the corridor acts as a wave-guide and channels the energy to the Rx through multiple reflections along the corridor. Higher order reflection is significant in the LOS conditions, while diffraction and scattering around the vicinity of the Rx play an important role in the NLOS condition. The loss associated in the process of reflection depends on the surface roughness and the material property of the reflecting surfaces. The channel is not dominated by the strongest LOS component since it has low K-factor values most of the time. Multiple reflections along the corridor seem to affect the frequency selective nature of the channel when both terminals are at the same height. The azimuth spread is unaffected by the height of the Rx and is about 3 times smaller in the LOS condition than that in the NLOS condition. This suggests that the design of any equalisation technique, RAKE receiver, or antenna array based system need to differ in LOS and NLOS corridor scenarios.

ACKNOWLEDGEMENT

The authors would like to acknowledge the Mobile VCE (www.mobilevce.com) for the funding support of C. M. Tan.

REFERENCES

1. M. Haardt, “Efficient one-, two-, and multi-dimensional high-resolution array signal processing,” PhD. Thesis, ISBN 3-8265-2220-6, 1996.
2. R. S. Thomä, D. Hampicke, A. Richter, G. Sommerkorn, A. Schneider, U. Trautwein, W. Wirnitzer, “Identification of time-variant directional mobile radio channels,” *IEEE Trans. Instrum. and Meas.*, vol. 49, pp. 357–364, April 2000.
3. L. M. Correia, *Wireless flexible personalised communications, COST 259 European co-operation in mobile radio research*, John Wiley, 2001.
4. J. F. Lafortune, M. Lecours, “Measurement and modelling of propagation losses in a building at 900 MHz,” *IEEE Trans. Veh. Tech.*, vol. 39, May 1990.
5. B. Fleury, “An uncertainty relation for WSS processes with an application to WSSUS systems”, *IEEE Trans. Comm.,* vol. 44, December 1996.
6. M. P. Fitton, A. R. Nix, M. A. Beach, “A comparison of the RMS delay spread and coherence bandwidth for characterisation of wideband channels,” *IEE Colloq. Propagation Aspects of Future Mobile System*, October 1996.